LES OF ROTATING TURBULENT PIPE FLOW WITH TWO SUBGRID SCALE MODELS

Zhiyin Yang and James J. McGuirk
Department of Aeronautical and Automotive Engineering
Loughborough University
Loughborough LE11 3TU
U.K.

ABSTRACT

It has been shown experimentally that turbulence is suppressed gradually in a rotating pipe with increasing rotation rate due to the stabilizing effect of the centrifugal force. These experimentally observed phenomena are confirmed numerically using Large-Eddy Simulation (LES) by comparing not only mean velocity profiles but also turbulent intensity and Reynolds stresses at two different rotation rates. In addition, the performance of two different subgrid scale models, a dynamical model and the usual Smagorinsky model, has been assessed for the case of fully developed turbulent swirling flow.

A brief description of the numerical methods used is presented. Particular attention has been paid to the numerical treatment of boundary conditions at the centre-line.

INTRODUCTION

The computation of strongly swirling turbulent flow is a challenging area for turbulence modelling. It is well established that the conventional two equation k-ε model has been successfully applied to many engineering calculations but its performance becomes poor in certain situations including the presence of swirling flows (Nallasamy, 1987). Large-Eddy Simulation has become a very useful and powerful tool in turbulent flow computations and has been applied to more and more practical engineering problems with the advance of computing power and numerical techniques (Lesieur and Metais, 1996, Voke and Yang, 1995, Voke, 1997, Yang, 1997). However, the literature on LES work in the area of turbulent pipe flow is very limited. Unger and Friedrich (1991) reported, to our knowledge, the first LES of fully-developed turbulent pipe flow without swirl and the only LES predictions of fully developed turbulent pipe flow with rotation which we are aware of is that carried out by Eggels and Nieuwstadt (1993). Their numerical results compared reasonably well with the experimental data available at that time, which however lacked complete details of the Reynolds stress field and what was available was not measured in the fully developed flow zone. They also used only a Smagorinsky subgrid scale model in the simulation; how a dynamic subgrid scale model would perform in such a swirling flow case is unknown.

Imao and Itoh (1996) have recently measured not only mean velocity profiles but also turbulence intensity and Reynolds shear stress in fully developed turbulent flow in an axially rotating pipe. Their detailed measurements provide good validation data for numerical computations and also confirm that when rotation is added to the pipe the turbulence fluctuations are suppressed due to the stabilizing effects caused by the centrifugal force. The main objectives of this paper are therefore: firstly, to study fully developed turbulent pipe flow by LES, in particular to examine the effects of swirl driven by the rotating wall of the pipe and assess these predictions against the data of Imao and Itoh (1996); secondly, to assess the performance of two different subgrid scale models, a dynamical model and the usual Smagorinsky model, in the swirling flow case.

BASIC EQUATIONS

The momentum and continuity equations used in the present study are given below in a cylindrical polar co-ordinate system (overbar indicating the filtering of the instantaneous fields to give the resolved scale fields omitted in the following equations for simplicity):

$$\frac{\partial q_x}{\partial t} = -r\frac{\partial p}{\partial x} + \frac{\partial}{\partial x}\left(\tau_{xx} - \frac{q_x q_x}{r}\right) + \frac{\partial}{\partial r}\left(\tau_{xr} - \frac{q_x q_r}{r}\right) + \frac{1}{r}\frac{\partial}{\partial \theta}(\tau_{x\theta} - q_x w) \qquad (1)$$

$$\frac{\partial q_r}{\partial t} = -r\frac{\partial p}{\partial r} + \frac{\partial}{\partial x}\left(\tau_{rx} - \frac{q_r q_x}{r}\right) + \frac{\partial}{\partial r}\left(\tau_{rr} - \frac{q_r q_r}{r}\right) + \frac{\partial}{\partial \theta}\left(\tau_{r\theta} - \frac{q_r w}{r}\right) - (\tau_{\theta\theta} - ww) \quad (2)$$

$$\frac{\partial w}{\partial t} = -\frac{1}{r}\frac{\partial p}{\partial \theta} + \frac{1}{r}\frac{\partial}{\partial x}(\tau_{\theta x} - wq_x) + \frac{1}{r^2}\frac{\partial}{\partial r}(r^2\tau_{\theta r} - rwq_r) + \frac{1}{r}\frac{\partial}{\partial \theta}(\tau_{\theta\theta} - ww) \quad (3)$$

$$\frac{\partial q_x}{\partial x} + \frac{\partial q_r}{\partial r} + \frac{\partial w}{\partial \theta} = 0 \quad (4)$$

Where q_x represents the axial flux ru (u is the axial velocity), w is the tangential velocity and q_r is the radial flux rv (v is the radial velocity) (note the density ρ has been set equal to 1.0 for convenience); the next section will discuss why the fluxes are introduced instead of the usual velocity components (u,v).

The stresses are given as follows

$$\tau_{ij} = 2(\nu + \nu_s)S_{ij} \quad (5)$$

where υ_s is the subgrid eddy viscosity

$$\upsilon_s = C\Delta^2 S \quad (6)$$

$$\Delta = \sqrt[3]{r\Delta\theta\Delta x\Delta r} \quad (7)$$

$$S = \sqrt{2S_{ij}S_{ij}} \quad (8)$$

and the strain rates S_{ij} in the present study using a cylindrical co-ordinate system are as follows:

$$\begin{bmatrix} S_{xx} & S_{xr} & S_{x\theta} \\ S_{xr} & S_{rr} & S_{r\theta} \\ S_{x\theta} & S_{r\theta} & S_{\theta\theta} \end{bmatrix} =$$

$$\begin{bmatrix} \frac{\partial q_x}{\partial x} & \frac{1}{2}\left[\left(\frac{\partial q_x}{\partial r} + \frac{\partial q_r}{\partial x} - \frac{q_x}{r}\right)\right] & \frac{1}{2}\left[\frac{\partial q_x}{\partial \theta} + r\frac{\partial w}{\partial x}\right] \\ S_{xr} & \left[\frac{\partial q_r}{\partial r} - \frac{q_r}{r}\right] & \frac{1}{2}\left[\frac{\partial q_\theta}{\partial r} + \frac{1}{r^2}\cdot\frac{\partial q_r}{\partial \theta} - \frac{q_\theta}{r}\right] \\ S_{x\theta} & S_{r\theta} & \left[\frac{1}{r}\cdot\frac{\partial q_\theta}{\partial \theta} + \frac{q_r}{r^2}\right] \end{bmatrix} \quad (9)$$

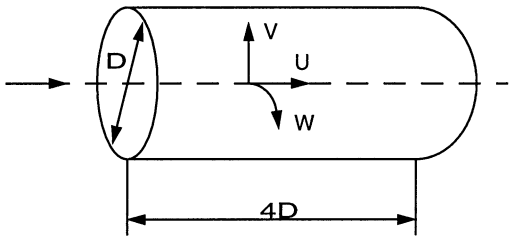

Fig. 1 Computational domain

C is taken to be 0.01 when the Smagorinsky subgrid scale model is used (with the Van Driest damping near the wall) and it is computed as follows when a dynamic subgrid scale model is employed:

$$C = \frac{\langle L'_{ij}M_{ij}\rangle}{\langle M_{kl}M_{kl}\rangle} \quad (10)$$

$$L_{ij} = T_{ij} - \hat{\tau}_{ij} = \widehat{\overline{u_i}\overline{u_j}} - \hat{\overline{u}}_i\hat{\overline{u}}_j \quad (11)$$

$$L'_{ij} = L_{ij} - \delta_{ij}L_{kk}/3 \quad (12)$$

$$M_{ij} = 4\hat{\bar{S}}\hat{\bar{S}}_{ij} - \widehat{\bar{S}\bar{S}}_{ij} \quad (13)$$

This is a standard procedure and details can be found elsewhere (Germano et al., 1991, Lilly, 1992); in the present simulation C is averaged in both streamwise and circumferential directions. However, this still cannot guarantee that C will not go negative although physically one can argue that this means backscatter. Numerically this can cause serious trouble when the total viscosity (sum of subgrid scale eddy viscosity and molecular viscosity) goes negative. In some regions, M_{ij} can be very small or may even approach zero, making equation (10) poorly conditioned and as a result of this C can be unrealistically large. In the current simulations the value of C has been monitored to check that it is not larger than 0.1 or less than 0. It has been found that the computed C in most of the simulation time and most of the computational domain is within this range.

NUMERICAL PROCEDURES

The above governing equations are discretised on a staggered mesh using finite-volume methods. The explicit second order Adams-Bashforth scheme is used for the momentum advancement except for the pressure term. The Poisson equation for pressure is solved using an efficient hybrid Fourier multigrid method described in more detail by Voke and Yang (1995).

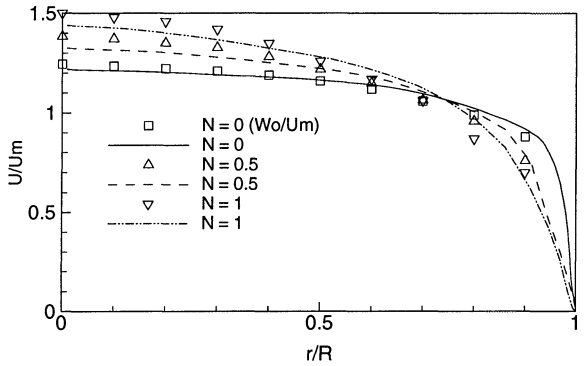

Fig. 2 Axial velocity, Lines--LES, Symbols--Exp. data

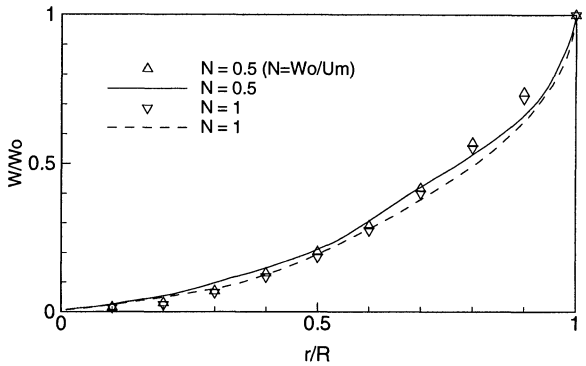

Fig. 3 Tangential velocity; Lines--LES; Symbols--Exp. data

Figure 1 shows the computational domain in the present study. The diameter of the pipe is D = 30mm and the length of the computational domain is 4D. In the circumferential direction the whole cross-section is simulated. The Reynolds number based on the mean axial velocity denoted as U_m (ρ*U_m*area=mass flowrate) and the pipe diameter is 20,000. All the dimensions and the Reynolds number have been chosen to match those of the experiments (Imao and Itoh, 1996). The simulations are carried out with 192*64*128 gridpoints (x, r, θ directions respectively) giving $Dx^+ = 30$; Dy^+ varies from 0.75 (nearest to the pipe wall) to 18 and Dz^+ varies from 0.7 (closest to the centre) to 36. This is a finer mesh near the wall than that used by Eggels and Nieuwstadt (1993).

Note that the small grid spacings of this fine mesh used near the pipe wall and the centre-line do cause time-step limitations in the explicit method used to solve the momentum equations.

Periodic boundary conditions are applied in the axial direction since the simulated pipe flow is fully developed. The same boundary treatment is applied in the circumferential direction at $\theta = 0^0$ and 360^0. On the pipe wall the usual no-slip boundary condition is applied.

However, due to the cylindrical co-ordinate system employed in the present study the governing equations contain a singularity at the centre-line of the pipe (r=0) which makes it difficult to specify boundary conditions for all velocity components at the pipe centre. Unger and Friedrich (1991) argue that no boundary conditions are needed since the grid surface area goes to zero and therefore the momentum and mass flux are zero too. The present work takes another approach to deal with this by solving for the fluxes (r times velocity components) instead of the velocity variables directly as shown in equations (1) - (4). Therefore at the centre-line zero is specified for all three variables employed in the equations. In addition to the singularity at the centre-line, the curvature of the cylindrical co-ordinate system can affect the time-integration. The time step is restricted by stability criteria to avoid numerical instabilities in all explicit time-integration schemes. Since the mesh size in the circumferential direction is proportional to r, it can become quite small towards the centre line. However, due to the present approach employing the fluxes as the variables, the minimum Dz^+ is 0.7 which is not too small and quite close to the minimum Dy^+. It has been found that, in these circumstances, there is no need for all the terms containing derivatives in the circumferential direction to be treated implicitly in time as has been adopted by Akselvoll and Moin (1996). The dimensionless time step used in the present study is 0.0002 (normalized by D/U_m) which is more or less the same as used for boundary layer transition studies (Voke and Yang, 1995, Yang, 1997).

The simulations are initiated from a specified axial velocity profile using a power law and random disturbances to mimic the turbulent fluctuations in all three directions. Since the random fluctuations generated in this way are large on small spatial scales and not well correlated, the viscous dissipation is large and this appears to remove the initial velocity fluctuations very effectively and to laminarize the flow. Therefore, the initial disturbances need to be stronger than the expected r.m.s level but not too strong as numerical instability may occur. There are alternative ways of avoiding such a rapid decay of artificially generated turbulence, for example reducing the viscosity initially. The simulations are run sufficiently long to reach a statistically stationary state before the statistics are collected. The final statistics are accumulated by spatial averaging in the homogeneous streamwise and circumferential directions and by time-averaging.

Three runs have been carried out in the present study, one with the pipe wall stationary and another two with the pipe wall rotating at different rates denoted by $N = W_o/U_m$ (W_o is the tangential velocity of the rotating pipe wall). Each simulation is usually run for 20000 time steps before the statistics are gathered and run for a further 40000 time steps to accumulate the statistics. One run takes about 80 CPU hours using one processor on a Cray-YMP machine.

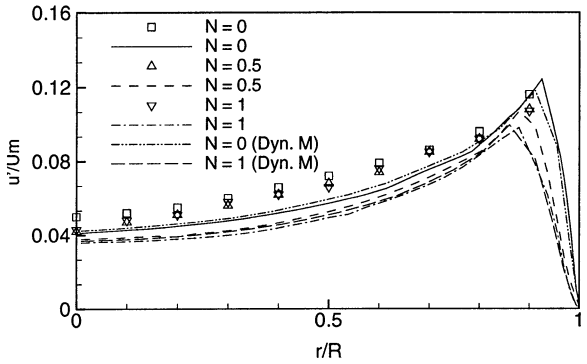

Fig. 4 Axial fluctuations; Lines--LES; Symbols--Exp. data

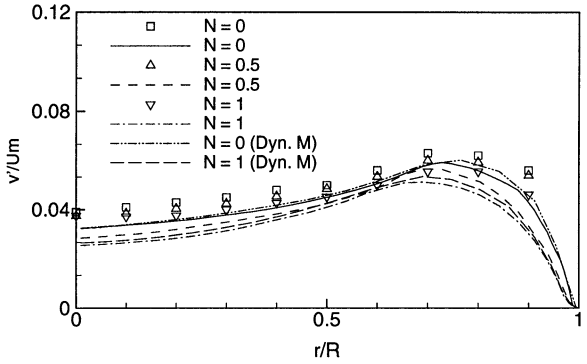

Fig. 5 Radial fluctuations; Lines--LES; Symbols--Exp. data

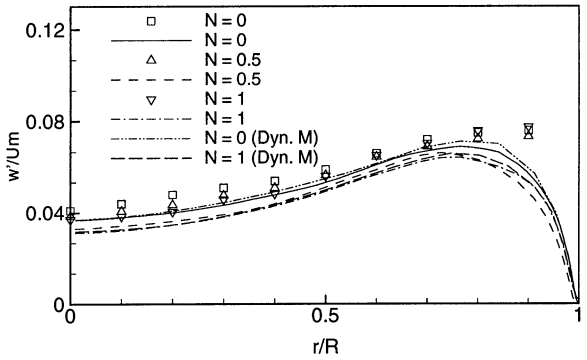

Fig. 6 Tangential fluctuations; Lines--LES; Symbols--Exp. data

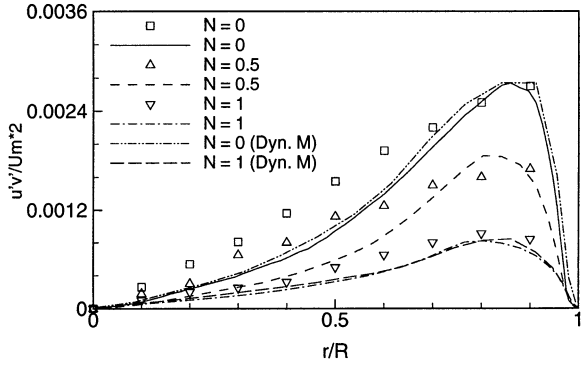

Fig. 7 Turbulent shear stress; Lines--LES; Symbols--Exp. data

RESULTS

Figure 2 shows the mean axial velocity profile normalized by the bulk averaged axial velocity U_m versus the radial position normalized by the pipe radius. The simulated results compare reasonably well with the experimental data for all three cases, N=0 (no rotation), N = 0.5 and 1.0 (pipe rotating). Both the experimental data and the simulated results show that when the pipe is rotating, the axial velocity increases near the centre and decreases near the wall, and the axial velocity profile gradually approaches a laminar shape with increasing rotation rate, due to the stabilizing effect caused by the centrifugal force. The experimental data show a slightly larger increase near the pipe centre.

The comparison between the simulated and measured tangential velocity profiles (normalized by W_0) is shown in Figure 3 for N = 0.5 and 1.0. Good agreement has been obtained between the numerical results and the experimental data for both cases. It can be seen from both the LES results and the experimental data that the tangential velocity profile is not a solid-body rotation type but similar to a parabolic distribution. It is well known that using a Reynolds-averaged approach with a linear eddy viscosity model would predict a linear forced vortex type profile. LES has produced better results in this case where turbulence modelling becomes difficult for strongly swirling flow. It is also worth pointing out that the profiles under the two rotation rates are more or less the same with little discrepancy between them and it can be said that the profiles are almost independent of rotation rate.

The above numerical results were obtained using the Smagorinsky subgrid scale model and the results obtained using a dynamical subgrid scale model (for cases N = 0 and 1) are almost identical and therefore have not been shown. However, there are some differences between predicted turbulence quantities obtained using different subgrid scale models as can be seen in Figures 4 - 7.

Following the practice by Imao and Itoh (1996) in normalising their experimental data, U_m is also used here as the parameter for normalizing turbulence intensity and Reynolds shear stress instead of u_τ (friction velocity). The

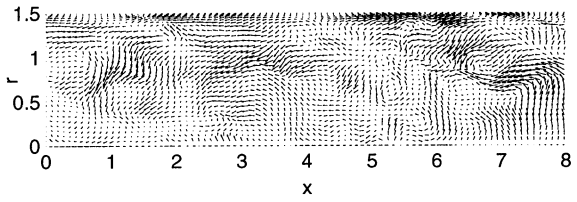

Fig. 8 (u', v') vectors at N = 0

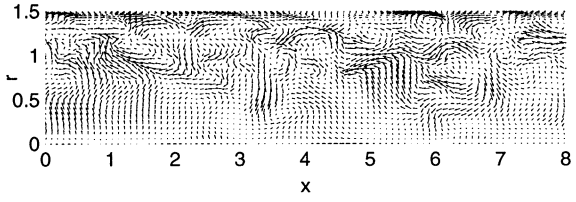

Fig. 9 (u', v') vectors at N = 1

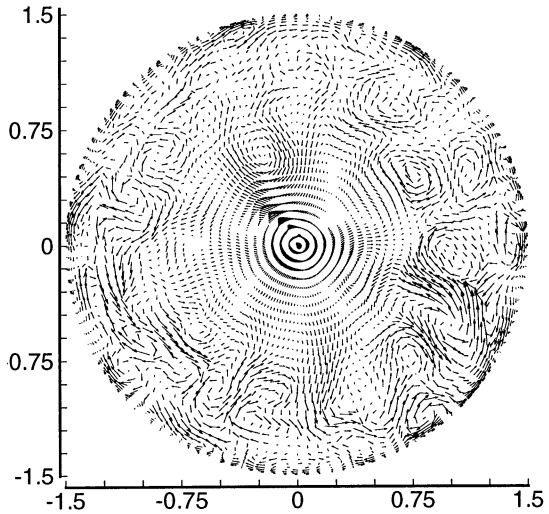

Fig. 10 (v', w') vectors at N = 0

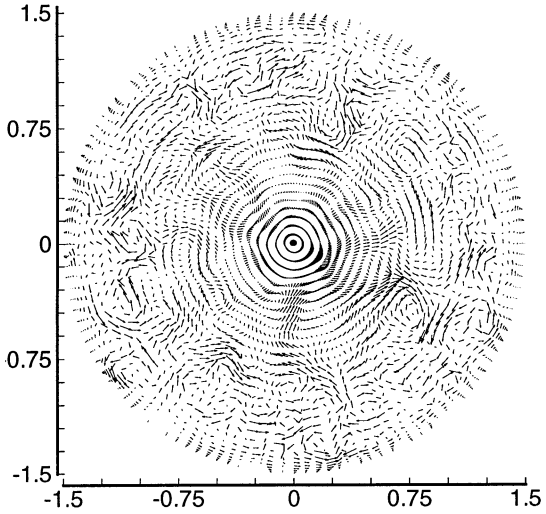

Fig. 11 (v', w') vectors at N = 1

reason for this is that when the pipe is rotating, the friction reduces due to the stabilizing effect as mentioned above, which means that u_τ decreases. If u_τ is used for normalization, Reynolds stress components become large when the pipe is rotating and hence it is difficult to tell the effect of pipe rotation directly. In addition, tangential shear stress exists when the pipe is rotating which also argues for U_m to be used as the normalization parameter.

Figure 4 shows the axial velocity fluctuations. The experimental data indicate that when the pipe is rotating the streamwise fluctuation decreases a little but not as much as in the LES results. The LES results clearly show that the fluctuation not only reduces when the pipe is rotating but also the peak of the fluctuation moves away from the wall. This is difficult to confirm from the experimental data as these are not available very near the wall when r/R is larger than 0.9.

The simulated peak values with both subgrid scale models are quite close to those of the experimental data but the results obtained using the dynamic subgrid scale show a slightly better overall agreement and the peak value especially is closer to the experimental data. However, the numerical results obtained by both subgrid scale models decrease slightly more quickly away from the wall.

The radial and tangential velocity fluctuations are presented in Figures 5 and 6. The numerical results follow the experimental data in that the fluctuations reduce slightly when the pipe is rotating with the radial component especially decreasing more compared with the other two components. This indicates that the radial fluctuation is the most suppressed. The predicted peak value locations for radial and tangential fluctuations move away from the wall when the pipe is rotating, similar to the axial component but the

movement is perhaps not so obvious. However, the simulated results from both subgrid scale models show that the predicted peak values, especially for tangential velocity, are slightly lower than those of the experiment. Again, the results from the dynamical subgrid scale model are slightly better.

The suppressing effect due to the rotation can be more clearly observed in Figure 7 which shows turbulent shear stress $\overline{u'v'}$ profiles. The LES results agree well with the experimental data in the near wall region but decrease more rapidly than the experimental data, similar to the normal stresses as discussed above. Both the LES results and the experimental data show a considerable reduction when the pipe is rotating. When the rotation rate changes from 0.5 to 1.0, the peak value of shear stress reduces to only about one-third of that without rotation. Again the simulated results from the dynamical subgrid scale are slightly better

Figures 8 and 9 show snapshots of turbulent velocity vectors (u',v') on an (x,r) plane at N = 0 and 1. It is difficult to tell the effects of pipe rotation from such a snapshot and hence the purpose of presenting these plots is not to compare the turbulent velocity vectors at different rotation rates but to present a general picture of the turbulent structures by examining the turbulent velocity vectors. It can be seen that elongated vortical structures exist near the pipe wall and a high intensity of fluctuations occurs in this region as well (this corresponds to the peak values shown in Figures 4 - 6). There are relatively weak fluctuations in the region near the pipe centre.

Figures 10 and 11 show snapshots of the turbulent velocity vectors (v',w') on an (r, θ) plane at N = 0 and 1. It can be seen from both plots that vortical structures exist in certain regions which indicates that most of the dynamics occur in those regions. Further away from the wall towards the central region there is much less activity. It is difficult to see the effects of pipe rotation from those snapshots but if one examines carefully the region very close to the wall then when the pipe wall is rotating there is slightly less turbulent fluctuations due to the suppression of radial fluctuations.

CONCLUSION

Large-Eddy Simulations with two subgrid scale models have been used to study fully developed turbulent pipe flow with different pipe wall rotation rates. The numerical results compare reasonably well with detailed experimental data and the performance of the dynamical subgrid scale model is only slightly better than that of the Samogrinsky model in the present study which may be attributed to the use of a fine mesh and the turbulent flow being fully developed. It is generally believed that a dynamic model would give better performance for many flow situations such as transitional flow, recirculating flow. The experimental observations that turbulence decreases with an increase in pipe rotation due to the stabilizing effect of the centrifugal force have been confirmed numerically by LES. The parabolic distribution of the mean circumferential velocity found in experiments is also reproduced by LES.

ACKNOWLEDGMENTS

The present results have been obtained as part of a BRITE-EURAM EU project on "Large Eddy Simulation Modelling For Lean Prevapourised Premixed Combustion".

REFERENCES

Akselvoll, K., and Moin, P., 1996, "Large-eddy simulation of turbulent confined coannular jets," *J. Fluid Mech.*, Vol. 315, pp. 387 - 411.

Eggels, E.G.M., and Nieuwstadt, F.T.M., 1993, "Larg-eddy simulation of turbulent flow in an axially rotating pipe," *Proceedings, 9th Symposium on Turbulent Shear Flows*, P310-1 - P310-4.

Germano, M., Piomelli, U., and Cabot, W.H., 1991, "A dynamic subgrid-scale eddy viscosity model," *Phys. Fluids A,* Vol. 3, pp. 1760 - 1765.

Imao, S., and Itoh, M., 1996, "Turbulent characteristics of the flow in an axially rotating pipe," *Int J. Heat and Fluid Flow*, Vol. 17, pp. 444-451.

Lesieur, M., and Metais, O., 1996, "New trends in large-eddy simulations of turbulence," *Annu. Rev. Fluid Mech.*, Vol. 28, pp. 45-82.

Lilly, D.K., 1992, "A proposed modification of the Germano subgrid-scale closure method," *Phys. Fluids A*, Vol. 4, pp. 633-635.

Nallasamy, M., 1987, "Turbulence models and their applications to the predictions of internal flows: a review," *Computer and Fluids*, Vol. 15, pp. 151-194.

Unger, F., and Friedrich, R., 1991, "Large eddy simulation of fully-developed turbulent pipe flow," *Proceedings, 8th Symposium on Turbulent Shear Flows*, pp. 19-3-1 ~ 19-3-6.

Voke, P.R., and Yang, Z., 1995, "Hybrid Fourier-multigrid pressure solution method for Navier-Stokes simulations," *Numerical methods for Fluid Dynamics V,* K.W. Morton et al., ed., pp. 615-6214.

Voke, P.R., 1997, "Flow past a square cylinder: test case LES2," *Direct and Large-Eddy Simulation II,* J.P. Chollet et al., ed., pp. 355-373.

Voke, P.R., and Yang, Z., 1995, "Numerical Study of Bypass Transition," *Phys. Fluids*, Vol. 7, pp. 2256-2264.

Yang, Z., 1997, "Large-eddy simulation of separated boundary layer transition," *Direct and Large-Eddy Simuation II,* J.P. Chollet et al., ed., pp. 137-146.